Anal. Chem. **2000,** *72,* 349−356

An Instrument for Simultaneous EQCM Impedance and SECM Measurements

Bernhard Gollas, Philip N. Bartlett,* and Guy Denuault

Department of Chemistry, University of Southampton, Highfield, Southampton SO17 1BJ, United Kingdom

A novel combination of an electrochemical quartz crystal microbalance (EQCM) and a scanning electrochemical microscope (SECM) has been built. Unlike conventional EQCMs, the instrument described here allows rapid in situ measurement of the modulus of the quartz crystal's transfer function. Data analysis in the complex plane for the Butterworth−Van Dyke (BVD) equivalent circuit yields the real and the imaginary components R (damping resistance) and X_L (reactive inductance) of the crystal's electroacoustic impedance around its resonant frequency of 10 MHz. The influence of different tip shapes of an approaching microelectrode on the electroacoustic impedance of the quartz crystal was studied and found to be minimal for certain geometries. The capability of the EQCM/SECM instrument was tested in cyclic voltammetric plating/stripping experiments using a copper(I) chloride solution of high concentration in 1 M HCl. Four parameters, X_L, R, the substrate, and the tip current, can be recorded simultaneously. Depletion layer effects were observed and could be corrected for to yield accurate current efficiencies for potentiodynamic and potentiostatic copper plating. The amperometric response of the SECM tip positioned closely to the substrate reflects the concentration changes of electroactive ions in the diffusion layer of the substrate electrode.

The electrochemical quartz crystal microbalance (EQCM)[1−4] and the scanning electrochemical microscope (SECM)[5,6] have been used independently to study the redox behavior of thin films on electrodes. For the investigation of electroactive polymer films, each technique has its limitations. If combined into one instrument, however, both techniques can provide complementary in situ data on the electrochemical and rheological behavior of polymer films.

The electrochemical quartz crystal microbalance has found widespread use in the investigation of thin films since its invention in the mid-1980s.[7] In the absence of changes in solution properties, measurement of the quartz crystal's resonant frequency changes can provide straightforward mass information in in situ studies of rigid films. In cases where the density and viscosity of the contacting solution vary simultaneously with the mass of the rigid film, frequency measurements alone cannot differentiate between changes in solution and film properties. On the basis of a continuum electromechanical model, Martin et al. derived the electrical admittance expression for an AT-cut quartz crystal simultaneously loaded with a surface mass layer and a contacting Newtonian liquid.[8] The modified Butterworth−Van Dyke equivalent circuit model (Figure 1), which describes this electrical admittance expression, can be used to analyze admittance data of the EQCM in terms of surface mass and solution properties. The convenience of this equivalent circuit model lies in the fact that any admittance changes that arise from mass or liquid loading can be expressed in terms of changes in L and R of the unperturbed resonator.[8]

Admittance data can be measured with impedance analyzers such as HP 4192A and HP 4194A models. However, recording an impedance spectrum around the crystal's resonant frequency requires several seconds and is thus not suitable for electrochemical in situ studies on similar time scales. Muramatsu et al. introduced a voltage divider circuit for rapid measurement of the modulus of the transfer function.[9] The correct analysis of the input and output voltages in the complex plane together with an improved voltage divider circuit was presented by Calvo et al.[10,11] This method allows the in situ measurement of the transfer function modulus around the resonant frequency of the quartz crystal on the time scale of milliseconds during electrochemical experiments. Subsequent fitting of the analytical expression for the transfer function modulus to the experimental data yields the parameters for the BVD equivalent circuit model. Changes in the rigid surface mass m only influence the inductance L, whereas changes of the viscosity density product $\rho_l\eta_l$ (the subscript l denotes properties of the liquid) of the adjacent solution are reflected in both L and the damping resistance R.

Most redox and conducting polymer films, however, behave neither as rigid layers nor as ideally viscous (Newtonian) liquids

(1) Schumacher, R. *Angew. Chem., Int. Ed. Engl.* **1990**, *29*, 329−343.
(2) Buttry, D. A. In *Electroanalytical Chemistry*; Bard, A. J., Ed.; Marcel Dekker: New York, 1991; Vol. 17, pp 1−85.
(3) Buttry, D. A.; Ward, M. D. *Chem. Rev.* **1992**, *92*, 1355−1379.
(4) Ward, M. D. In *Physical Electrochemistry*; Rubinstein, I., Ed.; Marcel Dekker: New York, 1995; pp 293−338.
(5) Bard, A. J.; Fan, F. R. F.; Mirkin, M. V. In *Electroanalytical Chemistry*; Bard, A. J., Ed.; Marcel Dekker: New York, 1994; Vol. 18, pp 243−373.
(6) Mirkin, M. V. *Anal. Chem.* **1996**, *68*, 177A−182A.
(7) Bruckenstein, S.; Shay, M. *Electrochim. Acta* **1985**, *30*, 1295−1300.
(8) Martin, S. J.; Granstaff, V. E.; Frye, G. C. *Anal. Chem.* **1991**, *63*, 2272−2281.
(9) Muramatsu, H.; Ye, X.; Sakuhura, T.; Ataka, T. *J. Electroanal. Chem. Interfacial Electrochem.* **1992**, *322*, 311−323.
(10) Calvo, E. J.; Danilowicz, C.; Etchenique, R. *J. Chem. Soc., Faraday Trans.* **1995**, *91*, 4083−4091.
(11) Calvo, E. J.; Etchenique, R.; Bartlett, P. N.; Singhal, K.; Santamaria, C. *Faraday Discuss. Chem. Soc.* **1997**, *107*, 141−157.

10.1021/ac990796o CCC: $19.00
Published on Web 12/10/1999

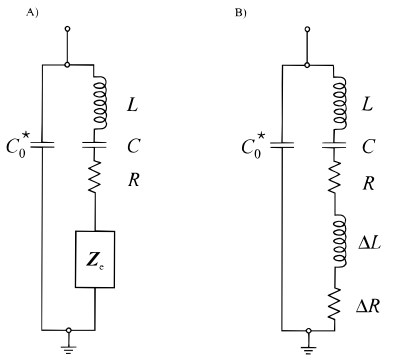

Figure 1. Modified BVD equivalent circuit model for a thickness shear mode resonator operating in contact with a liquid: (A) with complex motional impedance element $\boldsymbol{Z}_e$ (from ref 23); (B) with $\boldsymbol{Z}_e$ resolved into motional inductance and resistance and expressed as changes of the unperturbed resonator.

and therefore have to be treated as viscoelastic polymer films.[12] Electron transfer across the electrode/polymer interface causes a flux of counterions across the electrolyte solution/polymer film interface to maintain charge neutrality. These counterions are accompanied by solvent molecules and—in the absence of permselectivity—electrolyte salt. The change in composition of the polymer phase also involves polymer reconfiguration. In other words, in addition to mass changes, electrochemical processes in polymer films lead to changes in film thickness and viscoelastic properties, described by the complex shear modulus $\boldsymbol{G}$. The mechanical impedance for a one-dimensional analysis of a piezoelectric resonator with multiple nonpiezoelectric layers i, each of thickness d_i, density ρ_i, and wave propagation constant $\boldsymbol{k}_i = j\omega(\rho_i/\boldsymbol{G}_i)^{1/2}$, where ω represents the angular frequency of the resonator, was derived by Granstaff and Martin.[13]

Under conditions where additivity of the impedance contributions of the individual layers applies, the impedance of the viscoelastic film is

$$\boldsymbol{Z}_f = R_f + j\omega L_f \tag{1}$$

$$= R_f + jX_{Lf} = \frac{2\omega L_Q}{\pi\sqrt{\mu_Q\rho_Q}}[\rho_f\boldsymbol{G}_f \tanh(j\omega d_f\sqrt{\rho_f/\boldsymbol{G}_f})] \tag{2}$$

with

$$L_Q = \frac{h_Q{}^3\rho_Q}{8Ae_{26}{}^2} \tag{3}$$

$\mu_Q = 2.957 \times 10^{10}$ N m^{-2} is the elastic constant for piezoelectrically stiffened quartz, $\rho_Q = 2650$ kg m^{-3} is the density of quartz, $\boldsymbol{G}_f = G_f' + jG_f''$ is the shear modulus of the film (with the storage modulus G_f' and the loss modulus G_f''), h_Q is the thickness of the quartz, $e_{26} = 9.652 \times 10^{-2}$ C m^{-2} is the quartz piezoelectric stress constant, ρ_f is the film's density, and d_f is its thickness. The measured components of the electroacoustic impedance of the QCM at a fixed central frequency of 10 MHz, R_f and X_{Lf}, depend on four parameters G', G'', ρ_f, and d_f, where d_f is equal to $m_f/A_m\rho_f$, with m_f being the film's mass and A_m being the mass-sensitive area of the quartz crystal. Thus we can only determine two parameters, either the viscoelastic properties of the film or its mass and thickness, if the other two are known under all experimental conditions.

By combining a SECM with the EQCM, it is possible to overcome some of these limitations. Positioning the tip of a microelectrode close to the film's surface allows us to measure concentration changes of redox-active species crossing the film/solution interface.[14] Hence, we are able to identify fluxes of counterions during redox cycling and to assess their influence on the film's impedance parameters measured by the quartz crystal microbalance.

Three other combinations of an EQCM with a SECM have been reported.[15−17] Hillier and Ward used a single-potential control between substrate and microelectrode, where the tip acted as the counter electrode. The study was aimed at the radial sensitivity mapping of two different quartz crystals. Cliffel and Bard described a SECM/EQCM instrument under bipotentiostatic control, which they used for studies of silver and C_{60} films. Their EQCM part, however, only measures frequency changes and is thus not capable of distinguishing between rigid and nonrigid films or cases where mass and solution properties change simultaneously. Shin and Jeon described the use of the EQCM as a method of calibrating the tip−substrate distance in the SECM. Again they only measured the frequency change for the EQCM.

In designing the EQCM/SECM instrument, it is important to minimize the interaction between the SECM tip and the oscillating quartz crystal. Approaching a thickness shear mode resonator (TSR) with an ultramicroelectrode in a liquid can lead to perturbations of the quartz crystal's acoustic impedance. Usually the SECM tip is not positioned close enough to the substrate to cause interaction with the transverse shear waves radiated into the liquid from the oscillating crystal. These shear waves decay within 200 nm in aqueous solutions[18] for 10 MHz resonators. In addition to the transverse shear waves, however, longitudinal or compressional waves are generated by the oscillating crystal, because of a gradient in the in-plane surface displacement. Martin and Hager have shown that these compressional waves extend into the solution over distances of centimeters[19] and that the approach of a coplanar reflecting interface perpendicular to the shear motion of the quartz can lead to periodic variations of the TSR's response. It will be shown, however, that this effect is negligible for very small diameter SECM tips. In this paper, we report the design and application of a novel in situ combination of an EQCM and a SECM.

We have chosen the Cu(II/I/0) system to demonstrate the capabilities of the new in situ combination of techniques. Plating and stripping of copper in a concentrated Cu(I) solution lead to simultaneous changes of the rigid surface mass of the quartz crystal and of the viscosity density product of the solution in the diffusion layer. This was measured as changes in the electroa-

(12) Ferry, J. D. *Viscoelastic Properties of Polymers*, 3rd ed.; Wiley: New York, 1980.
(13) Granstaff, V. E.; Martin, S. J. *J. Appl. Phys.* **1994**, *75*, 1319−1329.
(14) Troise Frank, M. H.; Denuault, G. *J. Electroanal. Chem. Interfacial Electrochem.* **1994**, *379*, 399−406.
(15) Hillier, A. C.; Ward, M. D. *Anal. Chem.* **1992**, *64*, 2539−2554.
(16) Cliffel, D. E.; Bard, A. J. *Anal. Chem.* **1998**, *70*, 1993−1998.
(17) Shin, M.; Jeon, I. C. *Bull. Korean Chem. Soc.* **1998**, *19*, 1227−1232.
(18) Kanazawa, K. K.; Gordon, J. G. *Anal. Chem.* **1985**, *57*, 1771−1772.
(19) Martin, B. A.; Hager, H. E. *J. Appl. Phys.* **1989**, *65*, 2627−2629.

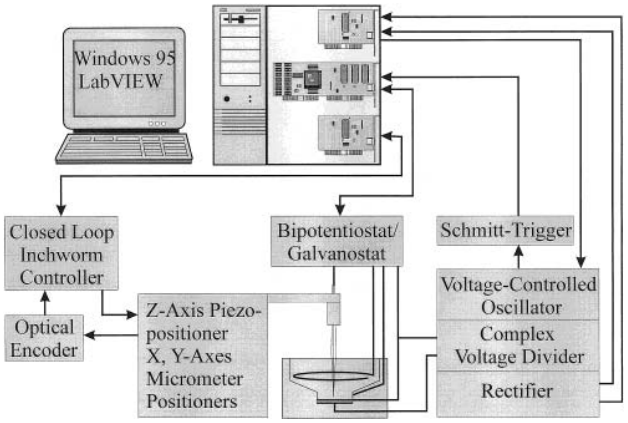

Figure 2. Block diagram of the in situ EQCM/SECM combination.

coustic impedance of the quartz, while the microelectrode sensed the concentration changes in the depletion layer.

EXPERIMENTAL SECTION

Chemicals and Solutions. Hexaammineruthenium(III) chloride (99%, Strem, Newburyport, MA) and potassium chloride (AnalaR, BDH) were used as received. Solutions were made with deionized water (a Whatman STILLplus system coupled to a Whatman RO 50) of 18 MΩ resistance. The 60 mM Cu(I) solution was prepared through the comproportionation reaction Cu(0) + Cu(II) = 2Cu(I) by bubbling Ar through the Teflon cell filled with a solution of $CuCl_2 \cdot 2H_2O$ (Fisons, Loughborough, U.K.) in 1 M HCl (AnalaR, BDH) in the presence of a Cu wire, which subsequently served as the counter electrode in the electrochemical copper experiments. The concentrations of Cu(I) and Cu(II) were checked by steady-state cyclic voltammetry at the SECM microelectrode in the bulk solution. The EQCM/SECM experiments were performed after the Cu(II) concentration had become negligibly low (≤0.5 mM).

EQCM/SECM Instrumentation. A block diagram of the EQCM/SECM instrument is shown in Figure 2. The EQCM circuit used consists of a voltage-controlled oscillator, a complex voltage divider, and a rectifier and is identical to the one described by Calvo et al.[11] The voltage ramp for the oscillator is generated from a LabPC+ DAQ board from National Instruments (Austin, TX) in a personal computer with an AMD K6 233 MHz processor running under Windows 95. The same board acquires the input and output voltages from the rectifier. For frequency baseline measurements, a Schmitt-Trigger and a counter on a second DAQ board (AT-MIO-16XE-10, National Instruments) were used. Unpolished, Au-coated (100 nm thickness, mass-sensitive Au disk area $A_m = 0.20$ cm^2, electroactive area $A_e = 0.22$ cm^2) AT-cut 10 MHz quartz crystals from ICM (Oklahoma City, OK) with 0.538 in. diameters were sealed between two O-rings and formed the bottom of the cell made from Teflon. The cell body contained holes to hold the saturated calomel reference electrode and to purge and blanket the electrolyte solution with argon. The cell lid had holes for the counter electrode, for the SECM microelectrode, and for a coiled glass tube, used for thermostating. All experiments were performed at 25 °C. Home-built 25 μm diameter Pt microelectrodes sealed in soft glass with insulator/Pt-disk radius ratios R_g of 4 and 90 were used as SECM tips (Figure 3).

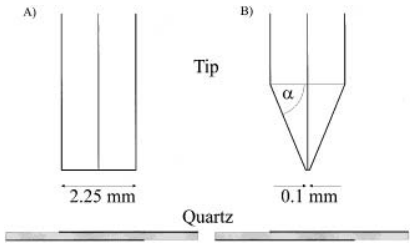

Figure 3. SECM tip shapes used in this study for 25 μm diameter Pt disks with insulator/disk radius ratios, R_g, of (A) 90 and (B) 4.

The positioner for the SECM microelectrode consists of an inchworm motor driven TSE-150 integral encoder stage for the *z* axis and two TS-75M stages with micrometer screws for the *x* and *y* axes (Burleigh Instruments, Fishers, NY). The inchworm driven stage for the *z* axis has a mechanical resolution of 4 nm. It is operated under closed-loop control with a model 6200 ULN inchworm controller (Burleigh Instruments) interfaced to the personal computer via a model 671 PC interface card (Burleigh Instruments). The optical encoder (Heidenhain, Traunreut, Germany) of the *z*-axis stage offers a resolution of 50 nm and an accuracy of 1 μm.

The potentials of the SECM tip and the Au (substrate) electrode were controlled by a home-built bipotentiostat/galvanostat. The substrate electrode was held at common ground. The bipotentiostat/galvanostat was fully computer controlled via the AT-MIO-16XE-10 DAQ board, which generated the potential waveforms and acquired the current data from the tip and the substrate electrodes. The programs were written in G with LabVIEW 4.1 (National Instruments).

After the experiments, the analytical expression of the transfer function modulus for the complex voltage divider with the BVD equivalent circuit was fitted to the experimental data.[10] This yielded the real and the imaginary components R and X_L of the quartz crystal's electroacoustic impedance. The nonlinear least-squares fitting program was written in Quick Basic 4.5.

Admittance Measurements. Admittance measurements of the quartz crystal at various tip−substrate distances in a 5 mM solution of $Ru(NH_3)_6Cl_3$ in 1 M KCl were measured with a HP 4291A impedance analyzer. The approximate tip−substrate distance was determined by approach curves before and after the admittance measurements had been carried out. Both curves were identical, which proved the absence of any drift during the measurement series. Admittance measurements were analyzed by fitting C_0* (static capacitance of quartz; the asterisk indicates the inclusion of contributions from wires and fixtures), L (inductance), and R (damping resistance) in the admittance expressions for the real

$$Y' = \frac{R}{R^2 + (\omega L - 1/\omega C)^2} \tag{4}$$

and imaginary

$$Y'' = \omega C_0^* - \frac{\omega L - 1/\omega C}{R^2 + (\omega L - 1/\omega C)^2} \tag{5}$$

parts to the data using the Levenberg−Marquardt nonlinear least-

squares algorithm in Origin 5.0 (Microcal, Northampton, MA). The value of the quartz compliance C was determined in an initial four-parameter fit and then held constant during fitting of the rest of the data.

RESULTS AND DISCUSSION

Interaction of the SECM Tip with the TSR. In the design of the EQCM/SECM instrument, it is important to take into account that the approach of the SECM tip can influence the response of the TSR. The generation of compressional waves by TSRs operating in liquids has been reported by Martin and Hager.[19,20] Subsequently, several other groups reported that acoustic interferometry can be performed with shear mode devices. In these experiments, periodic variations of the resonator's response were observed either by varying the temperature of the liquid between the resonator and an adjacent solid at a fixed distance[21] or by varying the distance.[22,23] In addition Schneider and Martin presented a model which quantitatively describes the periodic changes of the damping resistance R and the inductance L of the quartz crystal during acoustic interferometry experiments. The response of the quartz crystal was analyzed on the basis of a modified BVD equivalent circuit (Figure 1).

The additional electrical impedance $\boldsymbol{Z}_e$ represents the contribution of the contacting fluid to the total impedance of the quartz crystal[23]

$$\boldsymbol{Z}_e = \frac{N\pi[\boldsymbol{Z}_s(0) + P\boldsymbol{Z}_c(0)]}{4K^2\omega_s C_0 \boldsymbol{Z}_{so}^{(q)}} \tag{6}$$

N is the harmonic number, K^2 the quartz electromechanical coupling factor, ω_s the series angular frequency, and $\boldsymbol{Z}_{so}^{(q)}$ the quartz characteristic shear mechanical impedance ($\boldsymbol{Z}_{so}^{(q)} = (\mu_Q \rho_Q)^{1/2}$). The profile factor P is a measure of the gradient in the surface displacement. $\boldsymbol{Z}_c(0)$ and $\boldsymbol{Z}_s(0)$ are the surface mechanical impedances associated with compressional and shear wave generation, respectively[23]

$$\boldsymbol{Z}_s(0) = \boldsymbol{Z}_{so}^{(f)} = \left(\frac{\omega\rho_1\eta_1}{2}\right)^{1/2}(1 + j) \tag{7}$$

and for the case where the characteristic compressional impedance of the reflecting solid is much larger than that of the liquid[23]

$$\boldsymbol{Z}_c(0) \cong -j\boldsymbol{Z}_{co}^{(f)} \cot(\beta_c h) \tag{8}$$

with

$$\boldsymbol{Z}_{co}^{(f)} = \rho_1 v_C \tag{9}$$

and

$$\beta_c = \omega / v_c \tag{10}$$

$$h = \frac{n\lambda_c}{2} \quad (n = 1, 2, 3, \ldots) \tag{11}$$

where $\lambda_c = v_c/f$ and v_c is the compressional wave velocity in the fluid and f the frequency of the resonator. $\boldsymbol{Z}_c(0)$ is infinite, when $\beta_c h = n\pi$.

For a Gaussian profile (commonly used as an approximation to describe the shear amplitude of TSRs), the profile factor was explicitly calculated[23] as

$$P = \left(\frac{\lambda_c}{2\pi R_G}\right)^2 \tag{12}$$

where R_G is the radial falloff from the Gauss function

$$v_{X0}(x, z) = D \exp\left(-\frac{x^2 + z^2}{R_G^2}\right) \tag{13}$$

and D represents the peak amplitude. $\boldsymbol{Z}_e$ can be resolved into real and imaginary components and represented as changes of the motional resistance R and reactive inductance X_L of the unperturbed resonator[23] (Figure 1)

$$\boldsymbol{Z}_e = \Delta R + j\omega\Delta L \tag{14}$$

$$= \Delta R + j\Delta X_L \tag{15}$$

Figure 3 shows the two tip geometries used in our study. The large tip had a cylindrical shape (Figure 3A), whereas the small tip was beveled to a cone shape (Figure 3B). For the approach and retraction of the large tip (2.25 mm diameter), periodic variations of R and X_L are expected, due to constructive and destructive interferences of compressional waves reflected from the coplanar tip face plane. This is observed experimentally as shown in Figure 4. The data in Figure 4 were obtained by measuring the admittance of the quartz crystal around its resonant frequency with a HP 4192A impedance analyzer with the tip at fixed distances approximately above the center of the quartz crystal. The tip−substrate distance was varied in 5 μm steps for most of the approach and was decreased to 2 μm steps close to the substrate. The measurement was analyzed by fitting C_0*, L, and R in the admittance expressions for the real and imaginary parts of the BVD equivalent circuit to the data. Minima as well as maxima in Figure 4B are 80 ± 5 μm apart, which corresponds to approximately half of the wavelength for compressional waves in aqueous solutions at 10 MHz (λ = 150 μm in water). The periodic excursions can thus be attributed to the coupling of compressional waves, reflected by the coplanar face plane of the tip to the shear waves, both generated by the oscillating quartz crystal. For a rough estimate of the magnitude in the variation of the series resonance frequency f_s (or X_L), one has to take into account that $\boldsymbol{Z}_e$ has been integrated over the whole surface of the resonator in the study of Schneider and Martin. In our case, only a fraction of the compressional wave is reflected by the face plane of the

(20) Martin, B. A.; Hager, H. E. *J. Appl. Phys.* **1989**, *65*, 2630−2635.
(21) Tessier, L.; Patat, F.; Schmitt, N.; Feuillard, G.; Thompson, M. *Anal. Chem.* **1994**, *66*, 3569−3574.
(22) Lin, Z.; Ward, M. D. *Anal. Chem.* **1995**, *67*, 685−693.
(23) Schneider, T. W.; Martin, S. J. *Anal. Chem.* **1995**, *67*, 3324−3335.

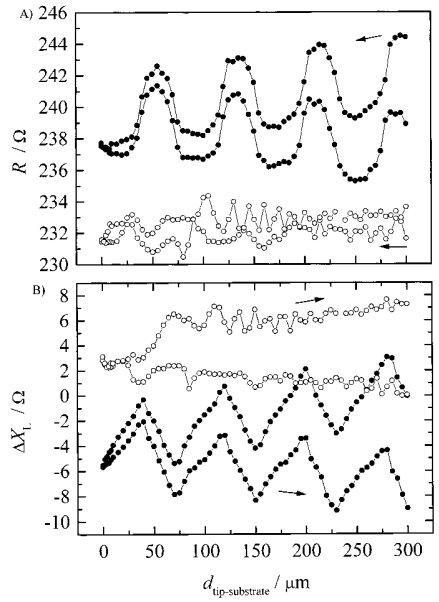

Figure 4. Impedance parameters of the quartz resonator as functions of the tip−substrate distance for large (•) and small (◦) SECM tips in 5 mM $Ru(NH_3)_6^{3+}$/1 M KCl.

large SECM tip, whose area is one-fifth of the area of the oscillating part of the quartz. If one assumes a similar radial falloff R_G for our similar device geometry in the equation for the profile factor P and a factor of $^1/_4$ for 10 MHz instead of 5 MHz resonant frequency, $f_s = [2\pi(LC)^{1/2}]^{-1}$, we arrive at frequency or reactive inductance excursions by a factor of 20 smaller than the 1.5 kHz or 140 Ω reported by these authors. As can be seen from the data in Figure 4B, this is indeed the case.

A second feature in Figure 4 is the underlying slope for R and ΔX_L during tip approach and retraction. A constant increase or decrease is observed for tips of both sizes and thus cannot be related to compressional wave interferences with the tips. The time for the slow admittance measurements exceeded 2 h for each of the tips. During this time, an appreciable volume of solvent evaporated from the open cell, causing an increase in electrolyte concentration and the viscosity density product of the solution. This is supported by the increase of the steady-state tip current for the $Ru(NH_3)_6^{3+/2+}$ couple measured in the bulk during approach curves before (21.7 nA) and after (28.3 nA) the admittance measurements with the small tip and the large tip (28.5 and 38.1 nA, respectively). The decrease in solution volume results in a decrease of the solution height above the crystal, and this in turn leads to the same kind of variation in compressional wave interaction between the liquid/air interface and the quartz crystal as observed for different tip distances (eqs 8−11).[22] The plots in Figure 4 are thus the result of the superimposed variations of the interferences between the quartz and the tip and between the quartz and the liquid/air interface, respectively.

For a cone-shaped tip of the general geometry shown in Figure 3B, compressional wave interferences depend at least on two parameters. The first, as in the case of the cylindrical shape, is the area of the coplanar face plane. The smaller the area, the smaller the extent of reflected compressional waves. The second parameter is the degree of beveling, expressed in the angle α. If α > 45°, the compressional waves are reflected upward and might

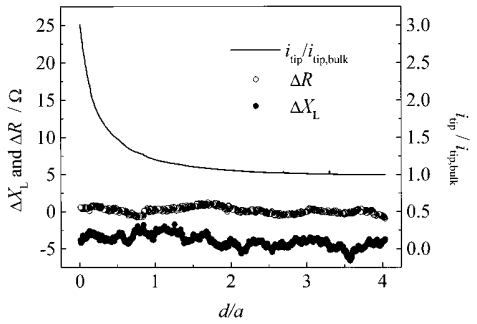

Figure 5. Variation of impedance parameters of the resonator during the SECM approach curve with a small cone-shaped tip in the positive feedback mode (5 mM $Ru(NH_3)_6^{3+}$/1 M KCl, $E_{tip} = -0.4$ V vs SCE, E_{sub} = open circuit, 0.1 μm/s approach speed).

cancel upon multiple reflections at the cell wall and the liquid/air interface. If α < 45°, the reflected compressional waves are directed downward. Depending on the exact value of α, a varying increase of compressional wave interference will result as the tip approaches the resonator surface. In the case of α = 45° and a vertical cell wall, compressional wave interference will depend on the distance between the resonator and the tip cone plus the distance between the cone and the cell wall. The reflectivity of the cell wall depends on the acoustic impedance ratio between the liquid and the cell wall material. The approach of our small tip (0.1 mm face plane diameter, α = 60−70°), whose approximate geometry is presented in Figure 3B, is also shown in Figure 4. Movement of the small tip toward and away from the surface does not cause periodic variations in R and L as seen with the large tip. The variations are nonperiodic and are on the order of only 1−2 Ω, which represents the accuracy limit of the measurement. The area of the part of the small tip, which is coplanar with the surface plane of the quartz crystal, is smaller than the oscillating area of the crystal by a factor of 10^4. The magnitude of the variation caused by the reflection of compressional waves from the small tip should therefore be negligible; even so, the cone of the small tip has some irregularities and is not as ideally cone-shaped as outlined in Figure 3B.

The results obtained from the admittance measurements with the impedance analyzer could be reproduced with our transfer function method. Figure 5 shows a SECM approach curve with a small tip (100 μm diameter) onto the center of the quartz crystal in the positive feedback mode with an approach speed of 0.1 μm/s, the tip potential $E_{tip} = 0.5$ V, and the substrate electrode at open-circuit potential in a 5 mM solution of $Ru(NH_3)_6^{3+}$ in 1 M KCl. Here the tip reduces $Ru(NH_3)_6^{3+}$ to $Ru(NH_3)_6^{2+}$, which is in turn oxidized back to $Ru(NH_3)_6^{3+}$ at the substrate electrode. The normalized tip current, $i_{tip}/i_{tip-bulk}$, shows the typical positive feedback response predicted when the tip substrate distance is less than 5 times the tip radius a. The impedance components R and X_L simultaneously recorded with our voltage divider circuit show no appreciable interaction between the tip and the oscillating quartz crystal.

In summary, it is possible to deduce design criteria for a minimal interaction between the TSR and the SECM tip. The resonator should have a planar−planar geometry,[22] a large radial falloff R_G (eq 12),[23] and a high fundamental resonance frequency to minimize compressional wave generation. Compressional wave

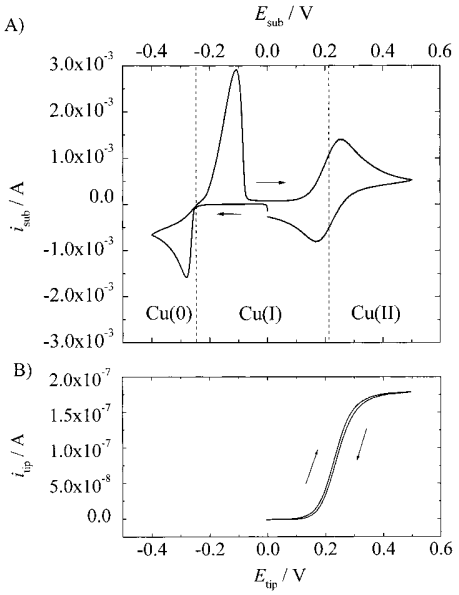

Figure 6. Cyclic voltammograms of 60 mM CuCl in 1 M HCl: (A) at the Au substrate electrode (A_{el} = 0.22 cm^2, v = 50 mV/s); (B) at the 25 μm diameter SECM tip in the bulk solution (v = 10 mV/s).

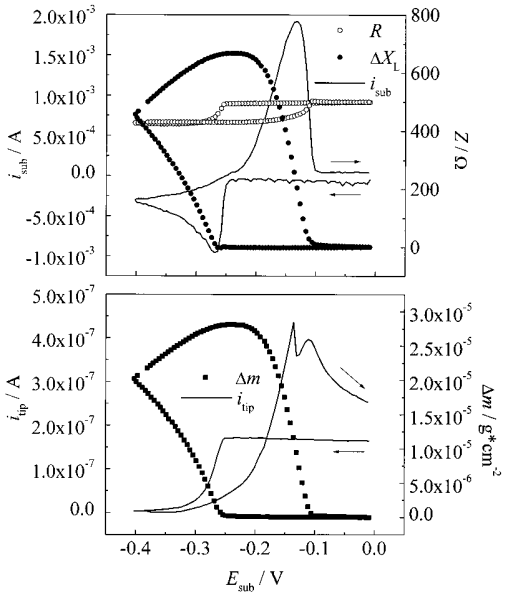

Figure 7. Cyclic voltammetry of 60 mM CuCl/1 M HCl at an Au substrate electrode (v = 10 mV/s, A_{el} = 0.22 cm^2) and simultaneously recorded quartz crystal impedance parameters R and ΔX_L (top) together with tip response, i_{tip} (25 μm Pt disk, E_{tip} = 0.5 V, approximately 2 μm above the substrate), and deconvoluted mass change, Δm (bottom).

interference can be further minimized by the use of a SECM tip with a small electrode radius, a, and small insulator radius, r_g. If the cell wall is vertical, the beveling angle α should be larger than 45°, to direct compressional waves reflected at the tip cone away from the resonator.

EQCM/SECM Experiments with a Rigid Film and Depletion Layer Effects. The upper part of Figure 6 shows a cyclic voltammogram for Cu(II/I/0) in 1 M HCl. Chloride ions stabilize the Cu(I) species as a $CuCl_2^-$ complex from neutral to low pH. This Cu system has the advantage of providing the solution redox couple Cu(II/I), as well as means to deposit a rigid film onto the substrate electrode by plating Cu(0). The solution couple can be used for SECM approach curves. This allows for easy positioning of the tip close to the substrate. A steady-state cyclic voltammogram of this solution couple for the tip far away from the substrate is shown in the lower part of Figure 6. Plating and stripping of a metallic copper film is a straightforward way of changing the mass of the quartz crystal and thus the imaginary part, X_L, of its electroacoustic impedance. The SECM tip positioned in the diffusion layer of the substrate electrode can simultaneously detect concentration changes of Cu(I) amperometrically in so-called substrate generator−tip collector experiments.

For generator−collector experiments, the tip was held at a fixed position approximately 2 μm above the substrate. This position was determined from an initial approach curve where the tip touched the substrate. Figure 7 shows four simultaneously recorded traces, the substrate current i_{sub}, the quartz crystal impedance parameters ΔX_L and R, and the tip current i_{tip} during potentiodynamic plating and stripping of Cu from the 60 mM Cu(I) solution. On the cathodic scan, the tip current falls to zero as all the copper in the thin layer between the tip and the EQCM is removed by plating as Cu(0) onto the EQCM. On the following anodic scan, the tip current shows a sharp oxidation peak followed by a broader oxidation peak corresponding to the detection of Cu(I) stripped from the EQCM electrode. Physical shielding of the substrate by the tip during the copper deposition means that less copper is deposited directly below the tip than in the surrounding region. During stripping, the copper stripped from the region directly below the tip is detected first, leading to the initial sharp peak in the tip current. At longer times the higher concentration of copper stripped from the unshielded part of the EQCM surface surrounding the tip diffuses radially to the tip, giving the second broader peak. The relative height and position of the two peaks and the general shape of the tip response depend on the tip−substrate distance, the insulator radius, r_g, and the scan rate of the cyclic voltammetric experiment. These significant features in the tip current curve could be reproduced by 2-dimensional digital simulation and will be reported in more detail elsewhere.[24]

In the EQCM response, in addition to an increase of X_L, we observe a decrease of R at the potential where plating of copper commences. At the beginning of the stripping process, R starts to increase again, and at the end of it, the initial value of R is restored.

These changes are attributed to the depletion and regeneration of Cu(I) during plating and stripping. The sensitivity of the EQCM toward viscosity and density changes of the bulk liquid was first reported by Kanazawa and Gordon[18] and Bruckenstein and Shay.[7] Recently, Lee et al. reported that composition changes in the depletion layer during redox processes of solution redox couples at high concentrations likewise influence the response of EQCMs.[25] They used standard finite difference methods to simulate the time-dependent concentration profiles of electroactive species in the diffusion layer. From these profiles, together with average

(24) Amphlett, J. L.; Denuault, G.; Gollas, B.; Bartlett, P. N. Manuscript in preparation.
(25) Lee, W.-W.; White, H. S.; Ward, M. D. *Anal. Chem.* **1993**, *65*, 3232−3237.

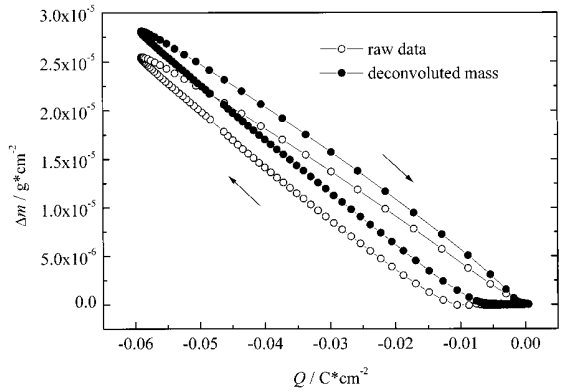

Figure 8. Plots of raw and deconvoluted mass data versus charge passed during the cyclic voltammetry experiment in Figure 7.

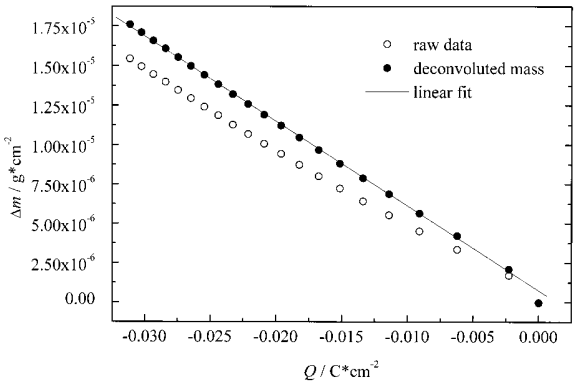

Figure 9. Plots of raw and deconvoluted mass versus charge passed during the potentiostatic plating experiment in 60 mM CuCl/1 M KCl solution (step from 0.0 to −0.3 V vs SCE; 10 s step time).

values of ρ_l and η_l in the layer, the authors calculated the expected frequency shifts using the Kanazawa−Bruckenstein equation for semiinfinite Newtonian liquid behavior

$$X_{\mathrm{Ll,Kan}} = R_{\mathrm{l,Kan}} = \frac{2\omega L_{\mathrm{Q}}}{\pi\sqrt{\mu_{\mathrm{Q}}\rho_{\mathrm{Q}}}}\left[\frac{\omega^{1/2}}{\sqrt{2}}\sqrt{\rho_1\eta_1}\right] \qquad (16)$$

The simulated frequency changes were in good agreement with the experimental results. On top of mass changes, we therefore expect to see appreciable changes of the viscosity density product in the depletion layer during plating and stripping of copper in a concentrated solution of Cu(I). From the above equation it can be seen that X_L and R depend equally on $\rho_l\eta_l$. Since the relative hardness of the Cu underlayer is much larger than the viscosity of the solution, the additivity condition for both impedance contributions applies.[13] This means that the mass of the Cu film can be calculated from ΔX_L by subtracting ΔR. A plot of the raw data, which corresponds to a frequency measurement, together with the deconvoluted mass versus the charge, is shown in Figure 8. Both sets of data represent closed loops, indicating the absence of irreversible electrode reactions. However, the raw data set is more curved in the initial plating part and during stripping, which reflects the influence of depletion layer effects. The plating part of the deconvoluted data is essentially linear except at the beginning of the process, where a slight upward curvature indicates a decrease in double-layer capacitance. The opposite curvature is observed during the more abrupt stripping process, showing that the double-layer capacitance of the gold electrode is restored. The plating data have a slope of 53.1 g F^{-1} mol^{-1}, which translates into a current efficiency of 84%. The data in Figure 8 were obtained by sweeping the potential in a cyclic voltammetry experiment. As a consequence, the charge contains a contribution from the double-layer charging current. This explains both the initial increase in charge without any initial mass increase and the hysteresis in the data. To obtain a more accurate estimate of the current efficiency, a potential step experiment was performed. In this case, the slope of the plot should not be distorted by double-layer charging since deposition of copper occurs at a constant potential. Figure 9 shows the raw data and deconvoluted mass data again plotted versus the deposition charge. While the raw data set shows a significant curvature, the set of deconvoluted mass data obeys excellent linearity after the initial double-layer charging. The linear fit has a slope of 51.8 g F^{-1} mol^{-1}, from which a current efficiency of 82% is calculated. This rather low current efficiency appears somewhat surprising. However, the measurements were validated by potentiostatic silver deposition experiments, which gave a current efficiency of 100%, within 5% experimental error. The low efficiency for the copper deposition is thus attributed to H^+ reduction as side reaction. Kruft et al. assumed that the adsorbed Cl^- layer on a Cu(111) single-crystal electrode causes an enhanced hydrogen evolution current to explain why the charge under the cathodic Cl^- desorption peak they observe in the cyclic voltammograms is larger than the charge under the corresponding anodic adsorption peak.[26]

In addition to depletion layer effects, a change in surface roughness could also contribute to R. Martin et al. reported that $\boldsymbol{Z}_e$ increases with surface roughness.[23,27] This effect is a linear combination of two components. For average surface roughnesses of $R_a > 0.15\delta$ ($\delta = (2\eta_l/\rho_l\omega)^{1/2}$) viscous damping of the shear wave by the liquid is proportional to R_a and hence the real surface area. It contributes equally to R and X_L (eq 14). For $R_a < 0.15\delta$, viscous damping is the same as that for an ideally smooth device. The second component is due to liquid trapped by the surface microstructure and behaves as a rigidly attached mass layer, thus increasing only X_L. Both contributions cannot be ruled out in our plating/stripping experiments. The first component is corrected for by subtracting ΔR from ΔX_L, leaving only the second component, a varying amount of entrapped liquid, as a source of error on Δm. However, since the initial surface roughness of the quartz crystals used in this study is at least 1 order of magnitude higher than the maximum thickness of the copper film (31 nm, calculated from Δm), surface roughness effects are expected to be small compared to the effect of solution composition changes near the surface.

CONCLUSIONS

A novel in situ combination of an EQCM and a SECM has been built. The instrument is capable of rapid measurements of the transfer function of the quartz crystal together with the current

(26) Kruft, M.; Wohlmann, B.; Stuhlmann, C.; Wandelt, K. *Surf. Sci.* **1997**, *377−379*, 601−604.
(27) Martin, S. J.; Frye, G. C.; Ricco, A. J.; Senturia, S. D. *Anal. Chem.* **1993**, *65*, 2910−2922.

transients of the substrate electrode and the SECM microelectrode. Subsequent analysis of the QCM data in the complex plane yields the electroacoustic impedance components of the quartz crystal during electrochemical processes. The influence of approaching SECM tips of two different geometries on the response of the resonator has been discussed on the basis of experimental results and theoretical considerations. Design criteria for the minimization of interactions between the tip and the resonator were given. Under optimal conditions, these interactions are negligible.

The instrument was tested by plating and stripping a copper film from a concentrated Cu(I) solution. Simultaneous changes for R and X_L were observed at the beginning of the plating process and during stripping. These changes were discussed in terms of depletion layer effects and changes of surface roughness. Depletion layer effects and the surface roughness component, which contributes equally to R and X_L, can be corrected for on the basis of models derived by Martin and co-workers[8,13,23] using the Kanazawa−Bruckenstein equation. The corrections are shown to yield linear mass charge data. The SECM tip, positioned close to the substrate, simultaneously detects concentration changes of Cu(I) amperometrically. The general shape of the tip response depends on the tip geometry and the tip−substrate distance as well as the time scale of the experiment. This additional information on ion fluxes across the substrate/solution interface can be useful in investigations of viscoelastic polymer films, where the impedance parameters R and X_L depend on the film mass and thickness as well as its shear modulus $\boldsymbol{G}$.

ACKNOWLEDGMENT

The authors are grateful to Dr. Roberto Etchenique, Universidad de Buenos Aires, for help in building the EQCM circuit and to Dr. John Owen for the use of the impedance analyzer. This work was funded by the Engineering and Physical Sciences Research Council, U.K., through Grant No. GR/K92306.

Received for review July 20, 1999. Accepted October 25, 1999.

AC990796O